

Article

Efficiency of the Vehicle Cabin Air Filters for Removing Black Carbon Particles and BTEX from the Air Intake

Tak W. Chan ^{1,2,*}, Marie Lee ³, Gary Mallach ⁴ and David Buote ²

- ¹ Climate Chemistry Measurements and Research, Climate Research Division, Environment and Climate Change Canada, 4905 Dufferin Street, Toronto, ON M3H 5T4, Canada
- ² Emissions Research and Measurement Section, Air Quality Research Division, Environment and Climate Change Canada, 335 River Road South, Ottawa, ON K1A 0H3, Canada; David.Buote@ec.gc.ca
- ³ Analysis and Air Quality Section, Air Quality Research Division, Environment and Climate Change Canada, 335 River Road South, Ottawa, ON K1A 0H3, Canada; Marie.Lee@ec.gc.ca
- ⁴ Water and Air Quality Bureau, Health Canada, 269 Laurier Ave West, Ottawa, ON K1A 0K9, Canada; gary.mallach@canada.ca
- * Correspondence: Tak.Chan@ec.gc.ca

Abstract: A laboratory study was conducted to evaluate 11 vehicular cabin filters (including electrostatic filters) in removing fine particles. Two filters with charcoal were also evaluated to understand their usefulness in removing five common volatile organic compounds, including benzene, toluene, ethylbenzene, and xylene isomers (BTEX). Filters were found to show considerably different particle filtration efficiencies (FE). Electrostatic filters were found to provide 20–60% better FE across all particle diameters (6–520 nm). For 6 nm particles, FE from 78 to 94% were observed (from the worst to the best filters), while at 520 nm, FE varied from 35 to 60%. The best group of filters provided 44–46% FE for capturing the most penetrating particles (100–300 nm), while the worst group of filters provided only 10–11% FE. The filtration behavior of nominal filters was typically stable (with respect to particle number, black carbon, and particulate matter mass) over the course of 1–2 years of usage. The benefits of the electrostatic filters were significant, but such advantages were observed to gradually dissipate over the course of about 1 year; by then, the electrostatic filter becomes no different compared to a nominal filter in terms of filtration behavior. Charcoal filters showed variabilities in removing BTEX, and removal efficiencies varied from 11 to 41%.

Citation: Chan, T.W.; Lee, M.; Mallach, G.; Buote, D. Efficiency of the Vehicle Cabin Air Filters for Removing Black Carbon Particles and BTEX from the Air Intake. *Appl. Sci.* **2021**, *11*, 9048. <https://doi.org/10.3390/app11199048>

Academic Editor: Elza Bontempi

Received: 9 September 2021

Accepted: 24 September 2021

Published: 28 September 2021

Keywords: in-cabin air quality; PM; black carbon; VOC; BTEX; filter efficiency

Publisher's Note: MDPI stays neutral with regard to jurisdictional claims in published maps and institutional affiliations.



Copyright: © 2021 by the authors. Licensee MDPI, Basel, Switzerland. This article is an open access article distributed under the terms and conditions of the Creative Commons Attribution (CC BY) license (<http://creativecommons.org/licenses/by/4.0/>).

1. Introduction

Toxicological and epidemiological studies showed that the short- and long-term exposure of various levels of particulate matter (PM) and black carbon (BC) is linked to acute respiratory system responses (e.g., allergy, asthma, and inflammation) and even mortality [1–5]. In addition, various volatile organic compounds (VOCs), such as benzene, are known human carcinogens [6,7]. Diesel and gasoline vehicles are known sources of PM, BC, and VOCs, and they contribute significantly to air quality and climate issues in urban areas as well as regions downwind of urban areas [8,9]. Canadians spend approximately 4–7% of their daily time in, on, or near-road locations, which is mainly associated with being in a vehicle [10]. Commuters who are riding on public transportation, driving in personal vehicles, or even walking or cycling in the vicinity of urban areas are exposed to various degrees of pollutants [11–13]. In-cabin exposure to particles and gaseous pollutants is a concern, particularly during rush hours on congested freeway or local roads.

A fibrous filter is a cost-effective means for removing airborne PM. Cabin filters in modern vehicles are typically designed to reduce concentrations of any incoming substances, such as pollen, mold spores, and road dust, preventing them from entering the heating ventilation air conditioning (HVAC) system of the vehicles. Studies showed that cabin filters are also effective for removing smaller particles by applying the vehicle recirculation ventilation setting [14–17]. At the filter, solid materials, such as PM and BC, can be removed by different filtration mechanisms depending on the size of the particles. Particles smaller than 0.1 μm are light enough that they do not follow air streamline when traveling. Instead, these particles undergo different degrees of random Brownian motion due to the thermal energy they process. The Brownian motion of these small particles is referred to as diffusion. When these particles pass through a filter, their random movements cause them to be removed by the filter fiber through interception. Particles larger than 1 μm are removed by impaction or interception because these particles are heavy enough that the momentum of the particles does not allow them to follow the air streamline through sharp turns [18,19]. Particles with diameter from 0.1 to 1 μm are too large to be efficiently removed by diffusion and too small to be effectively removed by impaction. These particles easily follow the air streamlines and are the most difficult to be removed by fibrous filters under most typical operating conditions, particularly for particles with 0.1–0.3 μm diameter. These particles are generally referred to as the most penetrating particles [20], and the filter FE are typically referred to the FE for removing these challenging particles.

While a typical cabin filter was expected to be ineffective for inorganic gases, research showed that activated charcoal filters are useful for removing various inorganic gases and hydrocarbons, which are often linked to symptoms and discomfort caused by diesel exhaust [14,21]. During recirculation mode, cabin air is forced through the vehicle cabin filter, while outdoor air intake is minimized. Although recirculation ventilation is effective in reducing in-cabin PM concentration, it quickly leads to an accumulation of passenger-exhaled carbon dioxide (CO_2) in the vehicle cabin. Current occupational exposure limits set for North American workplaces (e.g., ACGIH or NIOSH) for an 8 h weighted average is 5000 ppm. Meanwhile, the American Society of Heating, Refrigerating and Air-Conditioning Engineers (ASHRAE) standard on ventilation for acceptable indoor air quality recommends indoor CO_2 levels should not be greater than the ambient CO_2 level by 700 ppm, suggesting that the CO_2 level should be kept below 1000 ppm [22,23]. Depending on the in-cabin volume, fan speed, and number of passengers, in-cabin CO_2 concentration can easily build up to half of the current occupational exposure limit (i.e., 2500 ppm) in just 20–40 min under recirculation mode [24,25]. Therefore, while the maximum PM reduction inside a vehicle can be achieved by air recirculation, passengers cannot fully benefit from this in reality.

The filtration efficiency (FE) of the cabin filter changes over time depending on the nature of the filter and the loading amount captured by the filter. Theory predicts that the FE of a filter could increase over time due to the formation of dendrites [26,27]. When the first particle deposits on a filter fiber, there is an increased probability that other particles will impact this attached particle and be captured. This process eventually builds a chain-like structure called dendrites. The formation of dendrites changes the microstructure of the fibers, extending the fiber structure, and it provides an additional capture mechanism and thus improves the FE over time. Even though loaded filters could have a better FE than a new filter, eventually, continuously loading materials to a filter leads to filter clogging, increases the pressure drop across the filter, and reduces FE.

Other factors that influence filter FE include particle size and composition, and the filter nature. Emissions from diesel vehicles or the new direct injection gasoline vehicles contain a significant amount of BC particles, and these fine particles are in aggregate form. Depending on the operating condition of the vehicle, combustion particles could vary from 10 to 100 nm, but majority of the BC particles are about 60–80 nm [28–34]. Particles that are produced during a combustion process could pick up charges that are generated

Downstream of the fan is the cabin filter housing box, and air was forced through the cabin filter before exiting the housing unit.

To verify the fan speed, the ventilation flow rate of a Dodge Grand Caravan was measured by a hot wire anemometer and a pitot tube from one ventilation window (while all other ventilation windows were closed) at a time. The linear flow rate was converted to volumetric flow based on the estimated ventilation window area. In this case, the maximum ventilation flow rate of the test vehicle was estimated to be about 66.5 L/s. During the experiment, the blower was set to about 38.4 L/s, which is close to a setting that would be used during driving.

Two multi-hole sampling probes were installed: one located at the entrance of the cabin filter housing unit and the other located behind the cabin filter. Multi-hole probes were used to ensure a more representative sampling for both gases and particles from the tunnel.

2.2. Automotive Cabin Filters

A total of 11 cabin filters, including the original equipment manufacturer (OEM) cabin filter, were evaluated in this study (Table A1 in Appendix B). There are three categories of cabin filters, including 6 standard filters, 3 electrostatic fiber filters, and 2 charcoal non-electrostatic filters. The standard filters typically have a white appearance and paper-like texture, similar to the typical high-efficiency particulate air (HEPA) filter (Figure A2a; Appendix C). The charcoal filters have a similar surface texture compared to the standard filter but are grayish in color (Figure A2e; Appendix C). Some of the filters are advertised in the package to contain electrostatic fibers to improve the filtration efficiency of the filter. It is not possible to differentiate between the electrostatic and standard filters by their appearance alone (Figure A2c; Appendix C).

2.3. Generation and Measurement of BC Particles

The BC particle standards were generated by a miniature combustion aerosol standard (miniCAST) burner [41,42]. The miniCAST uses a co-flow diffusion flame of hydrocarbon to produce BC particles. The flame is quenched with dry nitrogen, which freezes the combustion process and stabilizes the BC particles produced during the combustion process. The diameter and concentration of the BC particles can be adjusted by changing the flow rate of the fuel (propane), oxidant (compressed air), and quenching gas (nitrogen).

During the experiment, the miniCAST was adjusted to produce 70 nm particles, approximating the diameter of observed vehicular BC particle emissions [28,33]. These particles were introduced into the flexible aluminum duct containing two turbulence mixing blades, which generated the necessary turbulence mixing. Then, particles passed through a mesh to produce a uniform particle concentration airflow before entering the cabin filter housing unit. Particles were alternatively sampled from either the pre- or post-filter locations through two multi-hole probes, which directed sampled air to the various particle instruments. Particle number size distributions (6–523 nm) were measured by the TSI Engine Exhaust Particle Sizer (EEPS) [43]. Real-time BC mass was measured by the Artium LII300 laser-induced incandescence (LII) [44,45], while particle mass was estimated using the Dekati mass monitor (DMM) [46]. In this study, each particle filtration experiment was done once on each filter.

The ambient concentration of BC and ultrafine particles observed from three Canadian cities (Toronto, Montreal, and Vancouver) during traffic rush hours was reported from the Urban Transportation Exposure Study (UTES) [47,48]. Median values of various pollutants, including the ultrafine particles, BC, and PM, observed at Toronto were used as target exposure concentration references (27,869 particles/cm³ UFP, 1.4 µg/m³ BC, 8.7 µg/m³ PM_{2.5}, and 12.6 µg/m³ BTEX).

2.4. BTEX Standard and VOC Analysis

In this study, 100 L standards of benzene, toluene, ethylbenzene, and xylene isomers (BTEX) were prepared and stored in a 15 L pressurized Summa stainless steel canister (Figure A1b; Appendix A). Table A2 (Appendix D) summarized the concentrations of the BTEX standards. These concentrations were chosen based on the exposure measurements obtained from Montreal during The Urban Transportation Exposure Study (UTES) [47,48] and were adjusted higher by a factor of 2 in order to simulate the concentration expected during rush hour on highly congested roads.

Before the experiment, the canister of BTEX standards was placed upstream of the aluminum duct, and the BTEX standard was released at 100 accm (actual cm³ per min) using a mass flow controller through a 60 cm long 1/8-inch diameter stainless steel tubing. Then, the standards passed through two turbulence blades to ensure they well mixed before entering into the cabin filter housing unit, without any filter installed. The BTEX standard was evaluated twice prior to the actual BTEX experiment. During the experiment, one of the three cabin filters (two charcoal filters and the OEM filter) was installed. Then, samples were extracted from two multi-hole probes that were positioned before and after the cabin filter simultaneously into two separated pre-vacuumed Summa stainless steel canisters, and the flow rate was restricted by a pre-calibrated needle valve. The absolute pressure inside the canister increased slowly over time as the BTEX was collected. When the absolute pressure inside the sample canister reached about 600 torr, the valve on the canister was shut and capped. Then, the canister was returned to the laboratory for VOC analysis. In this study, the BTEX experiment was done twice on each charcoal filter.

In this study, an in-house method similar to the U.S. Environmental Protection Agency (EPA) TO15 method was used to characterize the BTEX compounds, which is an automated cryogenic concentration technique [49]. In brief, an aliquot of air was first drawn from the Summa canister into a cryogenic pre-concentrator. Then, the trapped sample was released stepwise through a series of different temperature-controlled traps to separate the target VOCs from other air components (e.g., water, carbon dioxide, argon, methane), which were also present in significant amounts. The procedure concentrates the samples and improves the signal to noise ratio, allowing the ambient level VOCs to be detected with a low detection limit. The concentrated BTEX compounds were analyzed by capillary gas chromatography using low-resolution mass spectrometric detection.

3. Results and Discussion

3.1. Particle Standard Generation

The concentration and the size of the particles produced from the miniCAST were reasonably stable during the course of the experiment, and Figure 2 provides a typical time series of the particle number concentration, BC, and PM mass observed during one typical experiment. When switching between the pre- and post-filter locations, the particle number, BC, and PM mass concentrations all changed accordingly. Zeros on the EEPS and DMM were checked by sampling through HEPA filters periodically during which the particle number and mass both dropped to zero (top and bottom panels in Figure 2). This shows no drifting in the electronics over time, ensuring measurements were correct and consistent throughout the experiment.

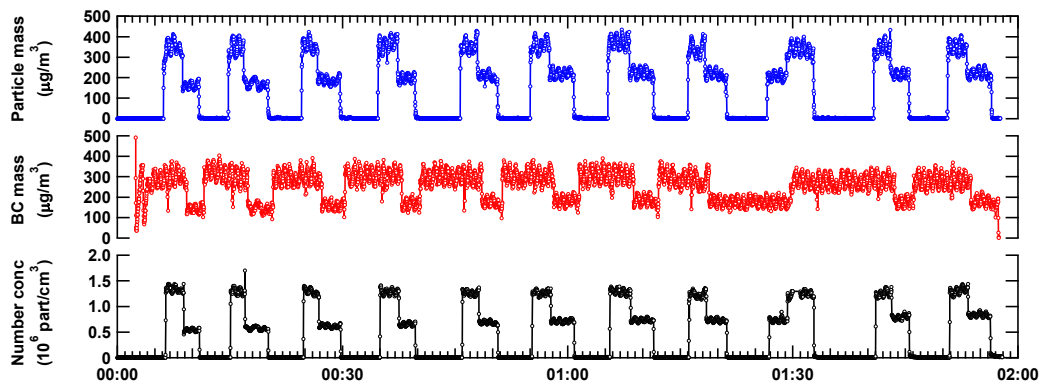


Figure 2. Example of the particle number concentration, black carbon (BC), and particulate matter (PM) mass time series from a typical experiment.

Experiments were performed on all 11 filters, and data were validated by reviewing all measurements thoroughly. Then, all data within each steady-state period were averaged. Figure 3a,b summarize the averaged particle number size distributions measured at the pre- and post-filter locations at various steady-state periods during one typical experiment. Figure 3a shows that the concentration and the size of the particles at the pre-filter location were relatively stable over the course of the experiment, which typically lasted between 1 and 2 h. The size of the particles measured at the post-filter location was consistent, but the particle number concentration pattern varied from experiment to experiment. In some cases, the particle number concentration was stable; however, in other cases, there was a progressive increase in the number concentrations over time (Figure 3b), indicating a loss of particle FE over time. Research on the loading behaviors of electrically active materials have observed that particle penetration through a filter may increase over time (i.e., decrease in FE) from a new state as material is loaded before filtration efficiency begins to improve [19,39]. More discussions on this will be given in Section 3.4.

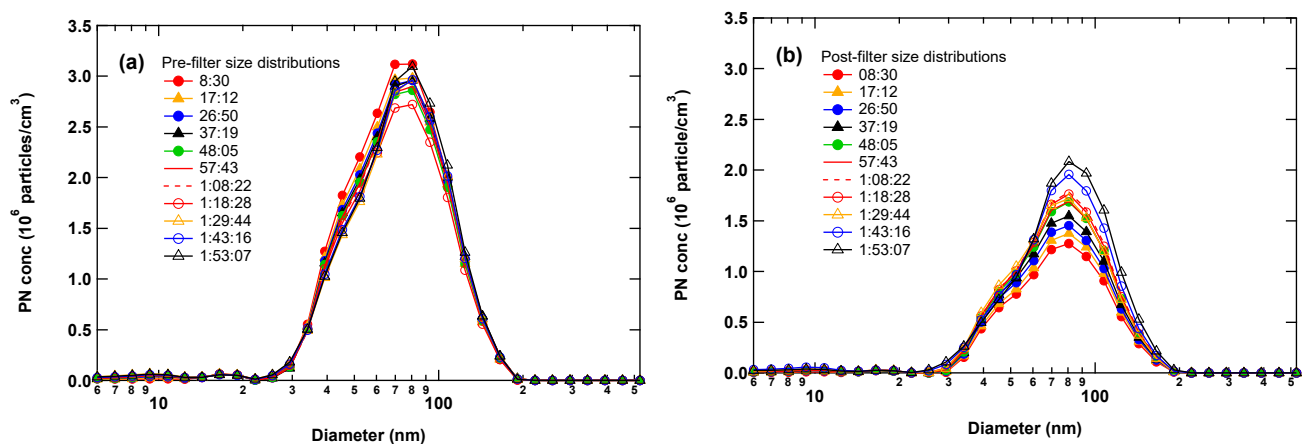


Figure 3. Example of the particle number size distribution measured at the (a) pre- and (b) post-cabin filter locations during a typical experiment.

3.2. Estimation of BC and PM Mass

As part of the quality control procedure, the measured BC and PM masses were validated by comparing to theory predictions. Combustion-generated soot particles have

fractal aggregate characteristics. The open structure of the particles creates extra drag on the particles. This results in decreasing effective density (defined as the ratio of the actual particle mass to the spherical volume of the particle calculated from mobility diameter) with increasing mobility diameter. Studies show that the effective density of combustion soot particles could vary from 2.5 g/cm^3 (for 10 nm particles) to 0.24 g/cm^3 (for 300 nm particles) [50–55]. Here, the mass of the BC particle, M_p (in μg), was estimated according to Park et al. [52]:

$$M_p = 6.05 \times 10^{-24} \cdot D^{2.34} \quad (1)$$

where D is the mobility diameter of the particle in nm. Figure 4a summarizes the variations of the calculated BC mass (based on Equation (1)) against the measured BC mass from the LII. The majority of the data points are in good agreement and fall within the region between the slope of 1 and 0.8. Part of the difference could be due to the fact that the particles produced from the current setting in this study are slightly different than those produced from Park et al. [52], which leads to differences in the mass mobility exponent (or sometimes referred to as fractal dimension), which affects the mass calculations. A study from Moore et al. [42] showed that particles generated from the miniCAST under various conditions contain different amounts of organic materials. Therefore, it is reasonable to expect that some of the organic materials fill up part of the void space in the soot aggregates when the aerosol stream is cooled, which also has an impact on the mass mobility exponent.

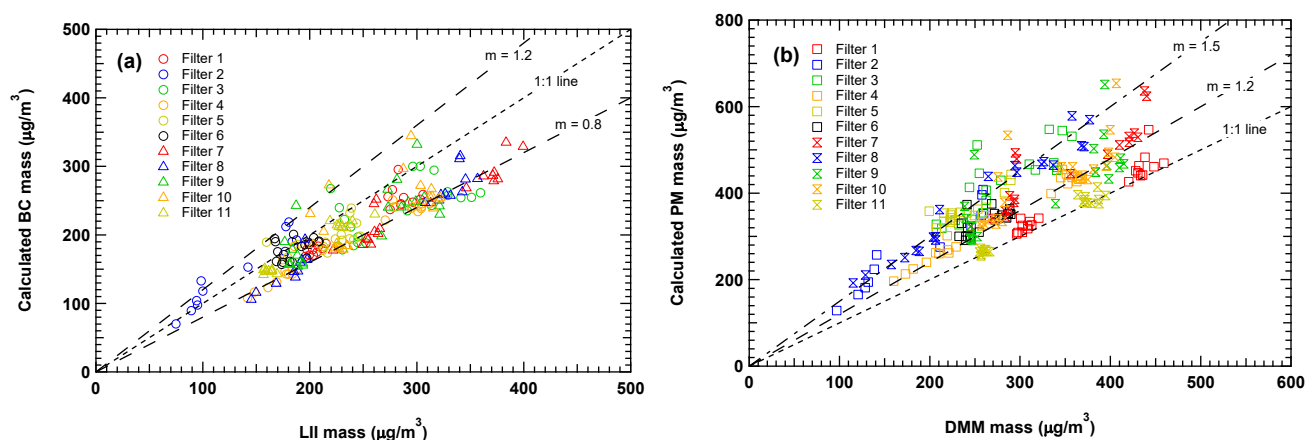


Figure 4. Comparison of the calculated (a) BC mass and (b) PM mass with the measured masses.

Particle mass was estimated here using the assumption of spherical particle and unity density (1 g/cm^3), and the results are presented in Figure 4b. Observations in Figure 4b show that the spherical particle assumption overestimates the particle mass by as much as 50% while a majority of the data points were overestimating by 20% due to the aggregate nature of the BC particles.

3.3. Particle Filtration Efficiency as a Function of Size

To determine the particle FE as a function of diameter, each individual averaged number size distribution observed at pre- and post-filter locations (i.e., Figure 3) were first fitted by a log-normal distribution to reduce measurement noise. Then, the pre- and post-filter fitted log-normal distribution measured at the two closest time periods were compared to determine the particle number (PN) FE over various diameters, $FE(D)$, which is defined as

$$FE(D) = \frac{N_{pre,Di} - N_{post,Di}}{N_{pre,Di}} \times 100\%, \quad (2)$$

where $N_{pre,Di}$ and $N_{post,Di}$ are the number concentrations at diameter D_i measured at the pre- and post-filter locations, respectively.

Figure 5 summarizes the PN FE as a function of particle diameter for all 11 filters in a box plot. In general, all FE curves possess a typical inverted V-shape, indicating the minimum FE at about 100 nm. This is similar to what would be predicted from theory and also consistent with the observations from other studies [38,56,57]. There were large variations in filtration performance among different filters. For example, filters 2, 4, and 8 had substantially better filtration performance than other filters. These filters were capable of removing 10 nm particles with close to 100% efficiency. They also provide FE up to 60% for 520 nm particles. The smallest FE of about 40% was observed for 100 nm particles as expected. Importantly, these filters had electrostatic properties, which also explain the high initial collection efficiencies of these filters compared to the non-electrostatic filters and the subsequent reduction in efficiency as the electrostatic charge was shadowed or reduced. Filters 5 and 6 had the worst performance as they typically provided 0% FE at 100 nm-sized particles. For all other sizes, the FE of these filters were typically 10–30% lower than the rest of other filters. The FE for the rest of the filters (i.e., 1, 3, 7, 9, 10, and 11) appears to fall in between the FE for the electrostatic filters and the underperforming filters groups.

Based on this preliminary analysis, the cabin filters were categorized into three groups. Group I represents the nominal filters (filters 1, 3, 7, 9, 10, 11), which represents what one would expect for a typical standard cabin filter. Group II is the electrostatic filters (filter 2, 4, 8), which have better FE than normal FE when new. Group III is the underperforming filters (filters 5, 6).

To understand the relative change in PN FE among Group II and Group III filters with respect to Group I, all PN FE for the same group were combined together to obtain the average PN FE as a function of sizes which are summarized in Figure 6. Results demonstrate that the presence of electrostatic fibers (red top) clearly enhance the particle capture across all sizes when compared to those without (black middle). For example, a 20% better FE was observed for 6 nm particles (Figure 7). The FE improvement slowly increased with particle size and reached 59% at 110 nm before it steadily declined to about 26% at 520 nm. Particles with diameter of about 100 nm are typically the most penetrating particle size in most typical sampling conditions because these particles are not heavy or light enough to be effectively removed by impaction and diffusion, respectively. This study shows that the electrostatic filtration mechanism can be an effective means to remove these particles from ambient air.

In comparison, Group III filters showed much worse performance compared to the Group I filters (Figure 6; blue bottom), especially for the most penetrating particle size around 100–200 nm which the FE for Group III filters were in general 60% less than that for Group I filters (Figure 7), or close to 0% in absolute FE (Figure 6). For the 520 nm particles, FE for Group III filters were typically lower than Group I filters by 28%.

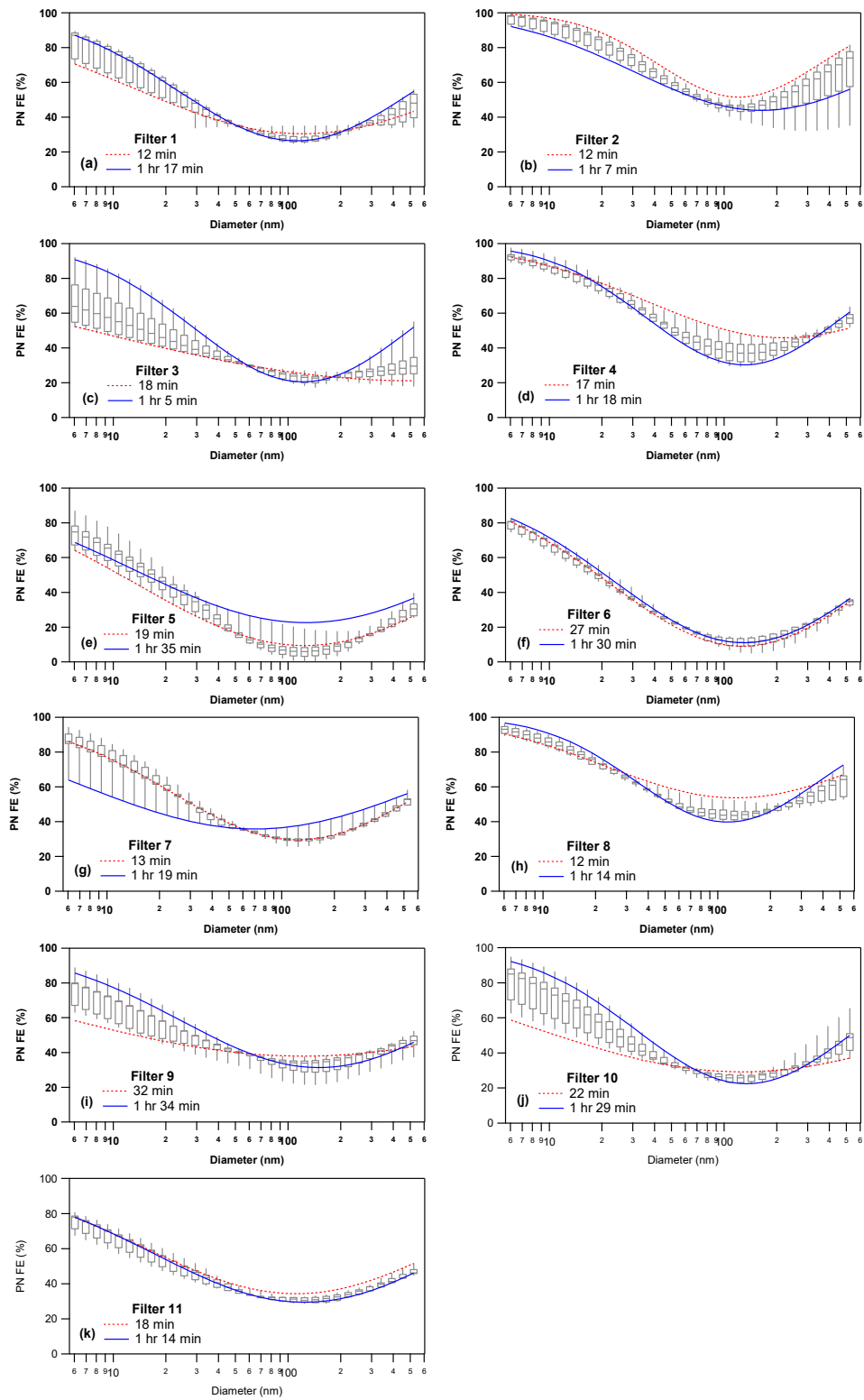


Figure 5. (a–k) Particle number filtration efficiency (PN FE) as a function of particle diameter for different cabin filters. Individual box represents the 30th, 50th, and 60th percentiles of the FE values over the course of the experiment, 20th and 80th percentiles are represented by the bottom and top whiskers, respectively. The dotted and solid curve represent the average PN FE at the beginning and the end of the experiment.

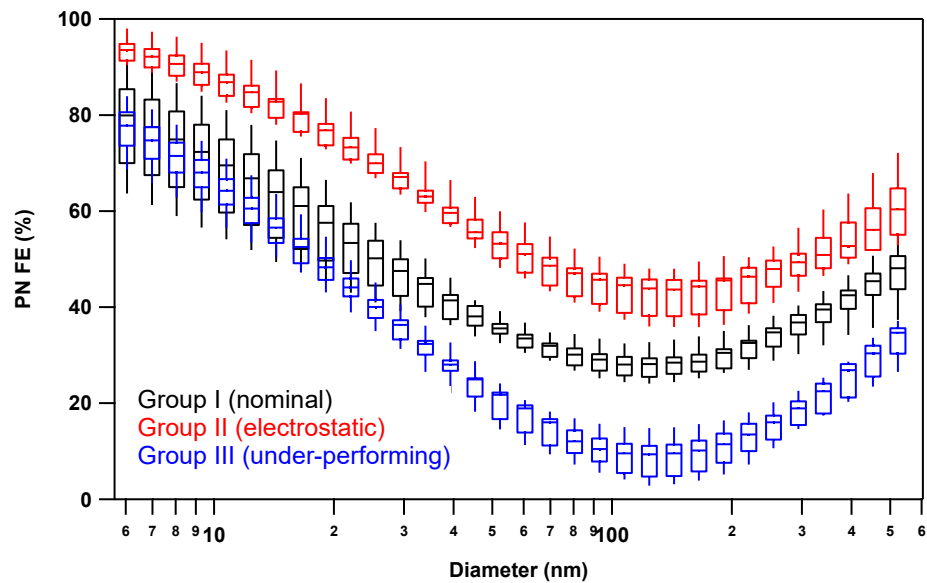


Figure 6. Average PN FE for the different filter groups. Each individual box represents the 30th, 50th, and 60th percentiles of the FE values over the course of the experiment, while the 20th and 80th percentiles are represented by the bottom and top whiskers, respectively.

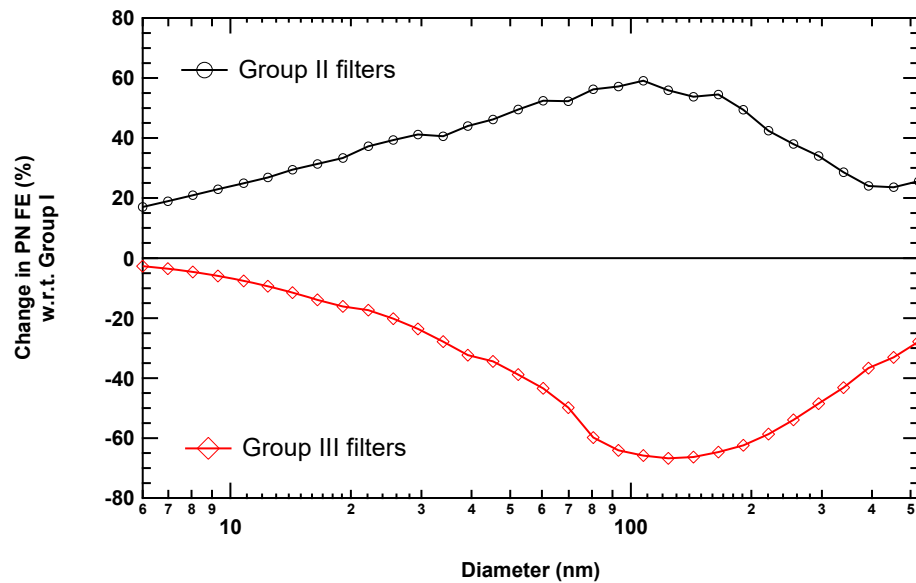


Figure 7. Percentage difference in PN FE for the Group II (electrostatic filters) and Group III (underperforming filters) with respect to Group I (nominal filters).

3.4. Particle FE Performance over Time

To determine the overall PN FE as a function of time, the particle number size distributions were integrated to obtain the total PN measured at both pre- and post-filter locations at various time points, which were then compared to determine how PN FE changed over time. The total accumulated particle number concentration introduced at the pre-filter location at various time points in an experiment was scaled based upon the on-roadway rush-hour exposure references from UTES, assuming 3 h of driving per day and ignoring weekend and weekday driving pattern [47,48]. Particles generated from the miniCAST contain a higher percentage of BC than ambient particles. Therefore, scaling the experimental time using BC mass results in more than double the time coverage. Since

the deposited BC mass on the cabin filter still contributes to the overall deposited mass on the filter, which will have an impact on FE, scaling the time with BC mass gives a more realistic scenario. After scaling, a typical experiment in this study represents about 300–800 days of filter usage.

Figure 8 summarizes the change in PN FE over time. Data are color coded based on the filter categories identified from the size-dependent FE. Results in Figure 8 show consistent behavior for different filters within the same group. Group I filters represent typical nominal filters, showing relatively flat FE behavior over the course of about 2 years of filter usage. Since observations in Figure 5 show that FE for different sizes did not change dramatically over the course of the experiment, the results in Figure 8 suggest that the relative FE for different sizes for Group I filters are stable over 2 years of usage in real life. Generally, FE for Group I filters varied from 30% to 40%. The formation of dendrites was expected to improve FE over time [27], but observations for Group I filters did not show this behavior. Fibrous filters typically have very low packing density in the range of 1–15% [19] to permit low pressure drop. Therefore, this also means that these filters typically have rather high filter capacity, and the amount of PM generated from this experiment obviously was not enough to significantly change any microstructure of the filter fiber to illustrate the improved FE caused by the formation of dendrites.

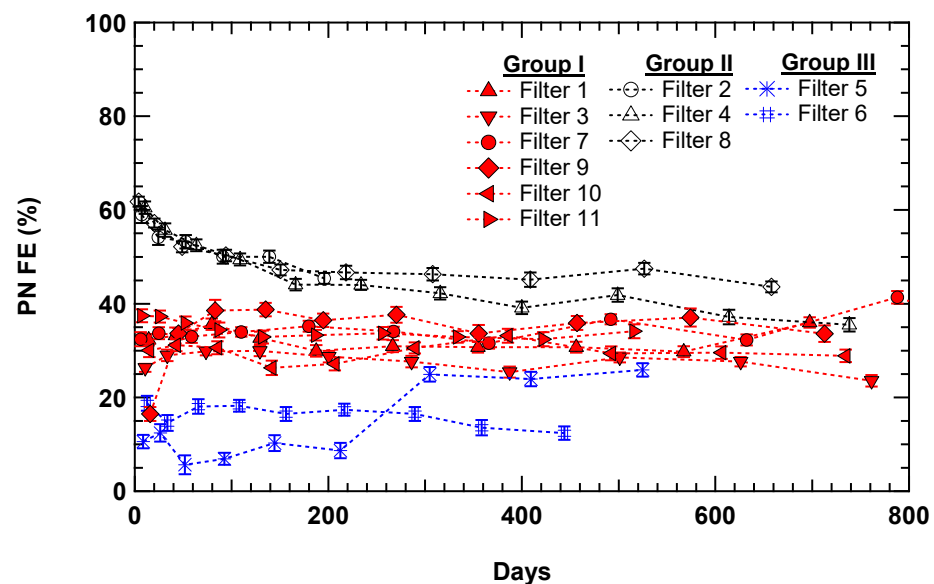


Figure 8. Particle number filtration efficiency over time for Group I (electrostatic filters), Group II (normal filters), and Group III (underperforming filters).

Group II filters had much higher FE (>60%) at the new state when compared to the nominal filters (FE of 30–40%). The high FE was due to the presence of the electrostatic charges on the filter fibers, which creates additional electrostatic attraction to help remove PM. The charges on the fibers typically do not dissipate over time and could be retained over years under favorable conditions. However, the charges could be lost for a number of reasons, such as high temperature, high humidity, or the deposition of organic liquid aerosol (e.g., oil or di(2-ethylhexyl)phthalate). The charges on the fibers can be neutralized when exposed to ionizing radiation, such as fine charged particles. The accumulation of dust on the fiber surface can mask the charges, creating a shadow effect and removing the benefit of electrically charged fibers [18,19,38,39]. It is beyond the scope and limitations of this study to determine the exact reason for the reduction of FE for Group II filters over time. However, since the FE of Group II filters showed a gradual reduction and approach to the typical FE of Group I filters, it is consistent with the expectation that FE reduction

could be due to the accumulation of dust. It is also possible that some of the BC particles generated from the miniCAST could carry charges, which could remove charges from the fibers. Once the charges from the filter fibers are neutralized or shadowed, the electrostatic filters lose their advantage and become a nominal filter and thus have comparable FE. This study suggests that the advantages of the electrostatic filters can be maintained for about 2 years of usage.

Group III filters are the underperforming filters. They have much lower FE that typically varied from 5 to 15%. Overall, the FE of these filters stayed relatively constant up to about one year time. The FE of one of the filters began to improve after about one year of usage with the FE approaching the nominal FE of the Group I filters. The improved FE was likely due to the accumulation of the dust and BC particles on the filter over time, which may have enhanced the filtration media to filter incoming particles. Note that this behavior only happened on one of the filters, and therefore, such improvement does not necessarily occur for all underperforming filters in a reasonable time scale.

3.5. Black Carbon and PM FE Performance over Time

The overall BC FE was determined by comparing the averaged pre- and post-filter BC concentrations (Figure 9). The overall patterns for all filter groups for BC are similar to that for PN. It is interesting to see a rapid improvement in BC FE for Group I filters that jumped from 20% at the new state to about 30% within a week in filter usage. BC particles are known to be in aggregate form, and the deposition of BC particles on filter fibers could enhance the formation of the dendrites, which could enhance the filtration of incoming particles [27].

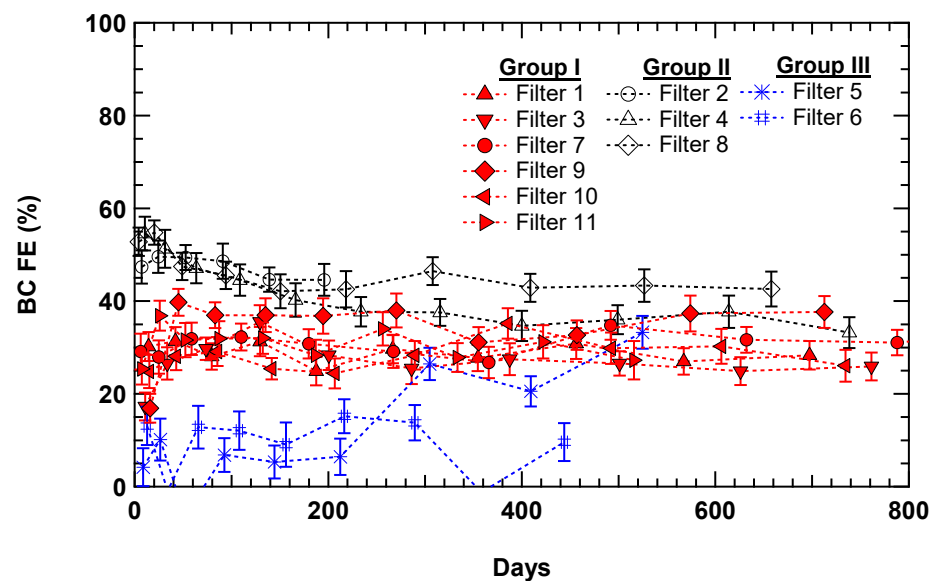


Figure 9. Black carbon mass filtration efficiency over time for Group I (normal filters), Group II (electrostatic filters), and Group III (underperforming filters).

Group II filters show similar exponential decay in BC FE over time as for the PN FE. This is due to the neutralization and shadowing of the charges on the filter fibers caused by the deposition of the BC particles. Similar to the PN results, it is expected that the advantage of the electrostatic filters will dissipate over about a year of usage. Group III filters show similar underperforming BC FE behavior as for PN FE, and the same conclusions discussed in PN FE can be applied in this case.

The overall PM FE was presented in Figure 10 and was calculated by comparing the averaged PM mass measured by the DMM at pre- and post-filter locations. The PM FE

results in Figure 10 were similar to the BC FE results because the particles generated from the miniCAST consisted primarily of BC. As such, the FE and related explanations also apply to the PM data.

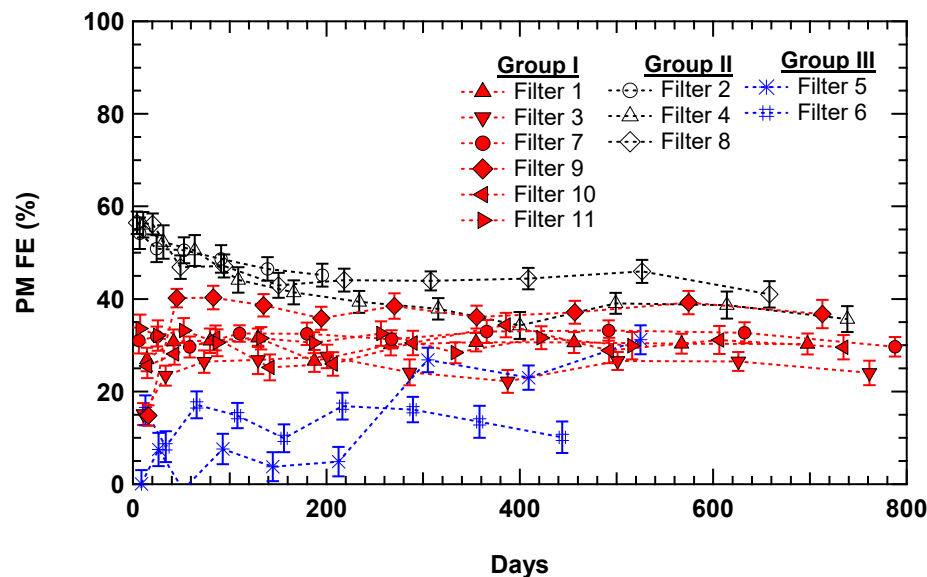


Figure 10. Particulate matter mass filtration efficiency over time for Group I (normal filters), Group II (electrostatic filters), and Group III (underperforming filters).

3.6. BTEX Removal Efficiency

Figure 11 shows the VOC concentration measured at the pre- and post-filter locations without a cabin filter installed. The excellent repeatability between the two repeats demonstrated the consistency in gas mixing created by the turbulence blades and the extraction through the multi-hole probes. However, observations also show a consistent difference in gaseous concentrations of 8–17% between the pre- and post-filter locations. The difference in gaseous concentration could be due to the sharp 90-degree bend in the filter housing unit (Figure 1) which is located right before the cabin filter location. This could create some eddies, but it also reflects the reality in an actual vehicle, which information will be taken into account in evaluating the efficiencies in various filters for removing BTEX.

Figure 12 summarizes the BTEX concentrations measured at the pre- and post-filter locations for a charcoal filter (ATP or Fram) and a non-charcoal filter (OEM). Since there is a consistent reduction in BTEX concentration between the pre- and post-filter locations (Figure 11), the averaged reduction amount was subtracted from the total reductions in BTEX concentrations for the all test filters in order to only reflect the change in BTEX concentrations due to the presence of a cabin filter. For the non-charcoal filter, the typical reductions in BTEX concentration were 3–5%. These changes are too small to be considered statistically significant, and they demonstrate that the non-charcoal filters have no impact on gaseous removal. In contrast, the two charcoal filters show significant removal of BTEX concentration, with one showing reductions of 11–17% with the other one showing reductions of 38–41%. These results suggest that even though there are variations in the BTEX removal efficiencies (RE) among different charcoal filters, charcoal filters are indeed useful in removing BTEX by typically more than 11%.

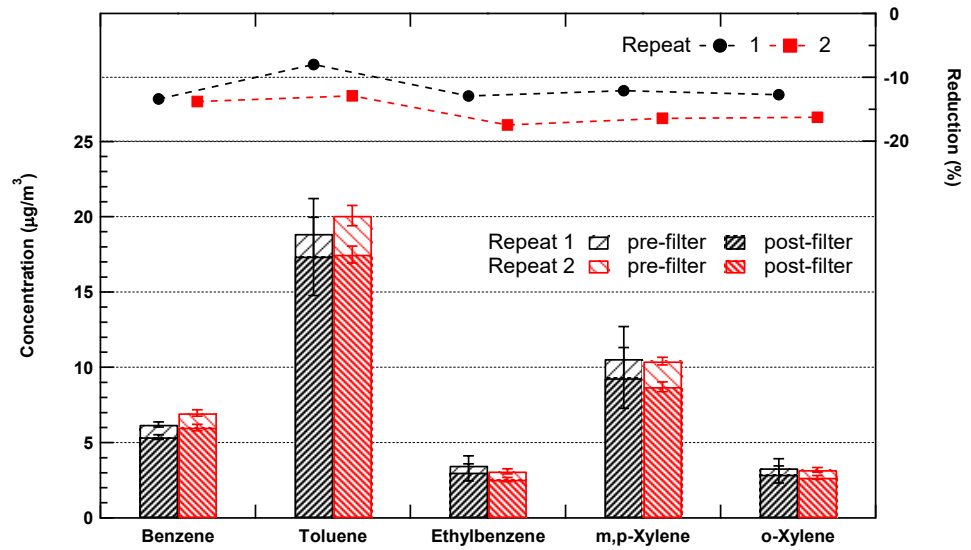


Figure 11. Measured BTEX concentrations at pre- and post-filter locations without cabin filters. Uncertainties are 95% confidence interval error estimates. Dotted lines indicate the reductions in BTEX concentrations at the post-filter location for the different repeats.

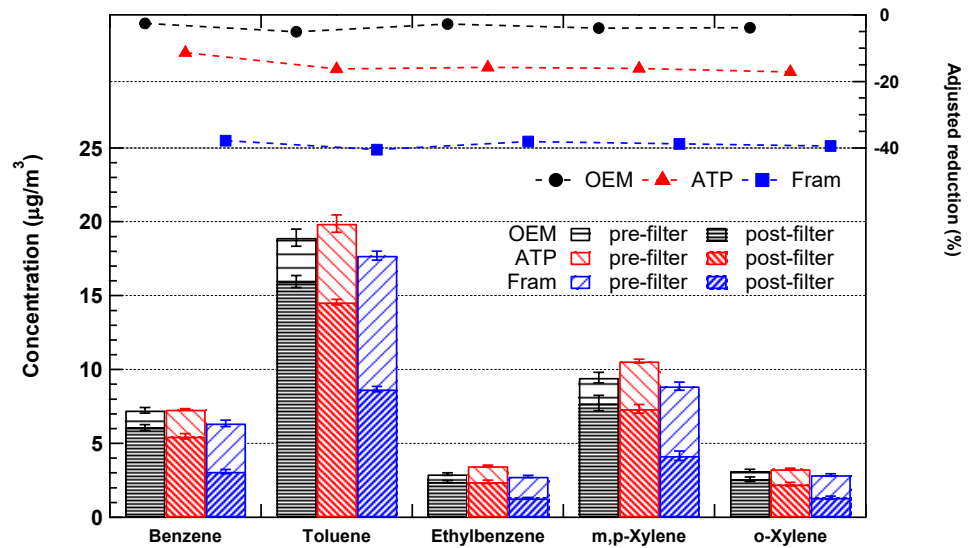


Figure 12. Measured BTEX concentrations at pre- and post-filter locations for various cabin filters.

4. Conclusions

Eleven vehicle cabin filters were evaluated to understand their FE in removing PM and BC from vehicular exhaust. All tested filters exhibit an inverted V-shape of FE with sizes (6–520 nm), and the most penetrating particle size was found to be 100–200 nm. Nominal filters generally offer 28–30% FE for 100–200 nm particles, 80% FE for 6 nm particles, and 48% for 520 nm particles. Electrostatic filters provide better FE across all tested sizes, showing 44–46% FE for 100–200 nm particles, 94% for 6 nm particles, and 60% for 520 nm particles. Two filters were found to underperform, showing only 78% for 6 nm particles and 35% for 520 nm particles. These filters only show 10–11% FE for 100–200 nm particles. The FE characteristics of all nominal filters did not change considerably, and the

FE (with respect to PN, BC, and PM) remained relatively stable (at 30–40% overall) within the course of the experiment, which can be translated to about 1–2 years of typical filter usage time. Electrostatic filters offer a significant improvement in overall FE with 60% at new state. The FE gradually declined over time and reaches the FE of nominal filters in about 1–2 years. The reduction in FE over time is attributed to the accumulation of dust and BC particles over time, which could shadow the charges on the fibers. The underperforming filters only offer less than 20% FE during the course of its usage, and in one case, the FE slightly improved after one year of usage likely due to the accumulation of dust and BC particles.

Experiments were also conducted to evaluate two charcoal cabin filters to understand their effect on removing BTEX. Observations demonstrated that charcoal filters were useful in removing BTEX compared to non-charcoal filters. One filter showed 11–17% of removal efficiency for BTEX, while the second filter showed 38–41%. Although not performed, it is expected that similar removal efficiencies could occur for similar VOCs. This study showed that the presence of charcoal extends the function of a cabin filter to provide additional gaseous removal ability in addition to PM removal.

Author Contributions: T.W.C. designed the experiment, constructed the laboratory setup, conducted the experiment, collect all gaseous and particle measurements, and analyzed the particle data and manuscript preparation. M.L. prepared the BTEX standard and led the laboratory VOC analysis. G.M. contributed to the study design and provided the cabin filters. D.B. constructed all the electrical connections. All authors have read and agreed to the published version of the manuscript.

Funding: This work was funded by the Emissions Research and Measurement Section of Environment and Climate Change Canada.

Data Availability Statement: The data presented in this study are available on request from the corresponding author.

Acknowledgments: The authors would like to acknowledge Peter Barton, Mark McCurdy, and Michel Souigny from Emissions Research and Measurement Section for providing technical suggestions to this study; Danny Wang from Analysis and Air Quality Section for providing scientific comments and suggestions to the VOC experiment; Chantale Dassylva from Departmental Project Management Office Division for providing access to a Dodge Grand Caravan for used in this project. The analysis, results and conclusion presented are those of the authors alone. The conclusions and views expressed do not necessarily, and should not be taken to, any endorsement from ECCC.

Conflicts of Interest: The authors declare no conflict of interest.

Appendix A

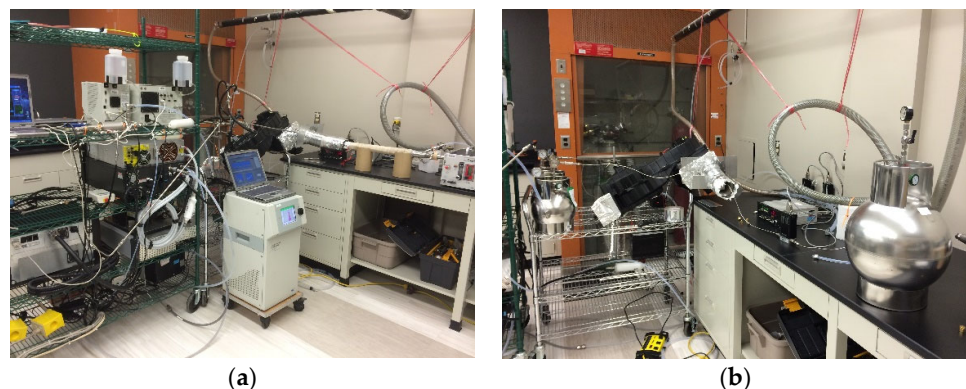


Figure A1. Photo on the left (a) shows the laboratory setup for the particle filtration efficiency experiment, while the photo on the right (b) shows the BTEX removal efficiency experiment setup.

Appendix B

Table A1. A list of the vehicle cabin filters for evaluation in this study.

Filter No.	Filter Brand	Filter Type
1	Fram Fresh Breeze	Charcoal
2	Denso	Electrostatic fiber
3	Napa	Standard
4	OEM	Electrostatic fiber
5	Pronto	Standard
6	Auto Extra	Standard
7	Mahle	Standard
8	Bosch	Electrostatic fiber
9	WIX	Standard
10	ATP	Standard
11	ATP charcoal	Charcoal

Appendix C

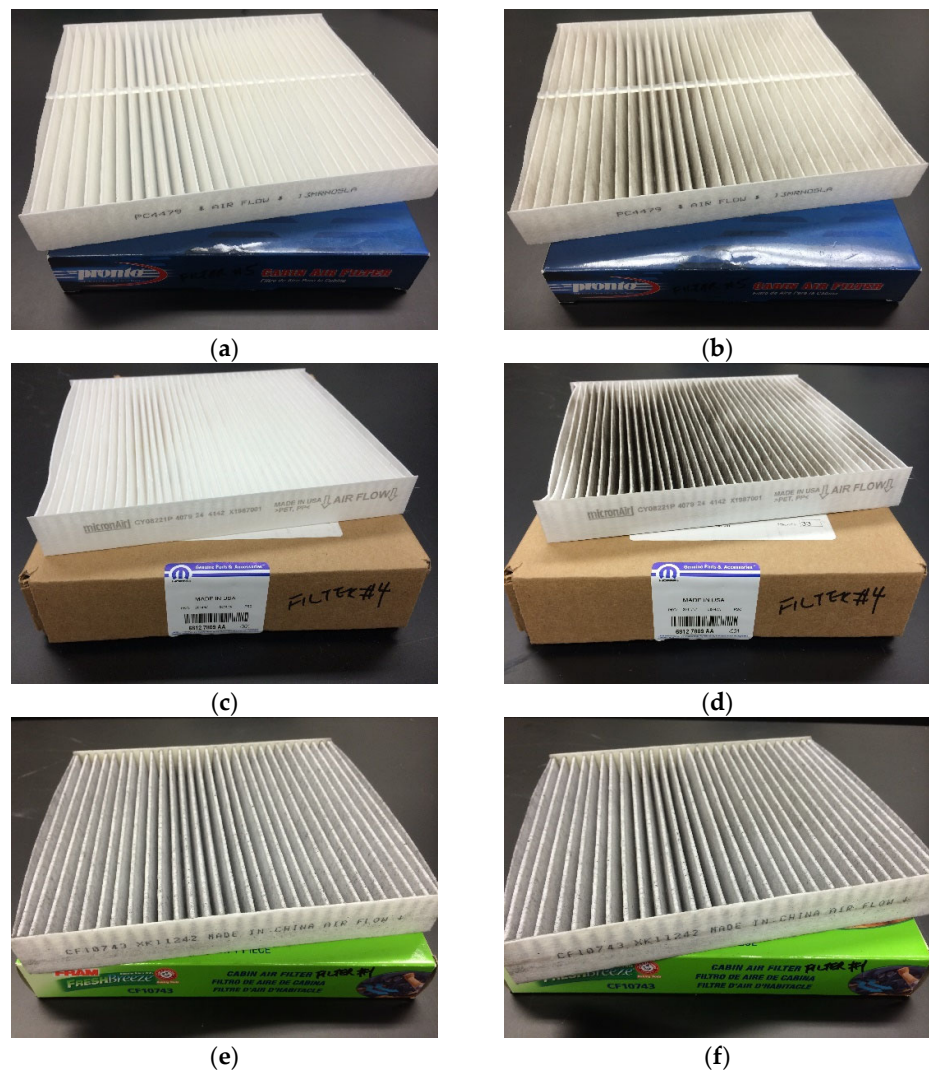


Figure A2. Photos showing a comparison of the appearance of (a,b) a standard filter, (c,d) an electrostatic fiber filter, and (e,f) a charcoal filter before and after the particle filtration efficiency experiment.

Appendix D

Table A2. Average concentration of the BTEX compounds in the standard.

Compound	Concentration in 100 Liter Air (ng/l)
Benzene	78,000
Toluene	229,000
Ethylbenzene	40,000
m,p-Xylene	118,000
o-Xylene	36,000

References

- Peters, A.; Skorkovsky, J.; Kotesovec, F.; Brynda, J.; Spix, C.; Wichmann, H.E.; Heinrich, J. Associations between mortality and air pollution in Central Europe. *Environ. Health Perspect.* **2000**, *108*, 283–287.
- Suglia, S.F.; Gryparis, A.; Schwartz, J.; Wright, R.J. Association between traffic-related black carbon exposure and lung function among urban women. *Environ. Health Perspect.* **2008**, *116*, 1333–1337.
- Ning, Z.; Sioutas, C. Atmospheric processes influencing aerosols generated by combustion and the inference of their impact on public exposure: A review. *Aerosol Air Qual. Res.* **2010**, *10*, 43–58.
- Wilker, E.H.; Baccarelli, A.; Suh, H.; Vokonas, P.; Wright, R.O.; Schwartz, J. Black carbon exposures, blood pressure, and interactions with single nucleotide polymorphisms in MicroRNA processing genes. *Environ. Health Perspect.* **2010**, *118*, 943–948.
- Thurston, G.D.; Burnett, R.T.; Turner, M.C.; Shi, Y.; Krewski, D.; Lall, R.; Ito, K.; Jerrett, M.; Gapstur, S.M.; Diver, W.R.; et al. Ischemic heart disease mortality and long-term exposure to source-related components of U.S. fine particle air pollution. *Environ. Health Perspect.* **2016**, *124*, 785–794.
- Knox, E.G. Childhood cancers and atmospheric carcinogens. *J. Epidemiol. Commun. Health* **2005**, *59*, 101–105.
- Wickliffe, J.K.; Stock, T.H.; Howard, J.L.; Frahm, E.; Simon-Friedt, B.R.; Montgomery, K.; Wilson, M.J.; Lichtveld, M.Y.; Harville, E. Increased long-term health risks attributable to select volatile organic compounds in residential indoor air in southeast Louisiana. *Sci. Rep.* **2020**, *10*, 21649.
- Malm, W.C. Atmospheric haze: Its sources and effects on visibility in rural areas of the continental United States. *Environ. Monit. Assess.* **1989**, *12*, 203–225.
- Bond, T.C.; Doherty, S.J.; Fahey, D.W.; Forster, P.M.; Bentsen, T.; DeAngelo, B.J.; Flanner, M.G.; Ghan, S.; Kärcher, B.; Koch, D.; et al. Bounding the role of black carbon in the climate system: A scientific assessment. *J. Geophys. Res. Atmos.* **2013**, *118*, 5380–5552, doi:10.1002/JGRD.50171.
- Matz, C.J.; Stieb, D.M.; Egyed, M.; Brion, O.; Johnson, M. Evaluation of daily time spent in transportation and traffic-influenced microenvironments by urban Canadian. *Air Qual. Atmos. Health* **2018**, *11*, 209–220.
- Duffy, B.L.; Nelson, P.F. Exposure to emissions of 1,3-butadiene and benzene in the cabins of moving motor vehicles and buses in Sydney, Australia. *Atmos. Environ.* **1997**, *31*, 3877–3885.
- Lee, K.; Sohn, H.; Putti, K. In-vehicle exposures to particulate matter and black carbon. *J. Air Waste Manag. Assoc.* **2010**, *60*, 130–136.
- Hudda, N.; Kostenidou, E.; Sioutas, C.; Delfino, R.J.; Fruin, S.A. Vehicle and driving characteristics that influence in-cabin particle number concentration. *Environ. Sci. Technol.* **2011**, *45*, 8691–8697.
- Rudell, B.; Wass, U.; Hörstedt, P.; Levin, J.O.; Lindahl, R.; Rannug, U.; Sunesson, A.L.; Östberg, Y.; Sandström, T. Efficiency of automotive cabin filters to reduce acute health effects of diesel exhaust in human subjects. *Occup. Environ. Med.* **1999**, *56*, 222–231.
- Zhu, Y.; Eiguren-Fernandez, A.; Hinds, W.C.; Miguel, A.H. In-cabin commuter exposure to ultrafine particles on Los Angeles freeways. *Environ. Sci. Technol.* **2007**, *41*, 2138–2145.
- Pui, D.Y.H.; Qi, C.; Stanley, N.; Oberdörster, G.; Maynard, A. Recirculating air filtration significantly reduces exposure to airborne nanoparticles. *Environ. Health Perspect.* **2008**, *116*, 863–866.
- Lee, E.S.; Zhu, Y. Application of a high-efficiency cabin air filter for simultaneous mitigation of ultrafine particle and carbon dioxide exposures inside passenger vehicles. *Environ. Sci. Technol.* **2014**, *48*, 2328–2335.
- Hinds, W.C. Filtration. In *Aerosol Technology: Properties, Behaviour, and Measurement of Airborne Particles*, 2nd ed.; John Wiley & Sons, Inc.: Hoboken, NJ, USA, 1999; Chapter 9, pp. 182–205.
- Wang, C.S. Electrostatic forces in fibrous filter—A review. *Power Technol.* **2001**, *118*, 166–170.
- Lee, K.W.; Liu, B.Y.H. On the minimum efficiency and the most penetrating particle size for fibrous filters. *J. Air Pollut. Control Assoc.* **1980**, *30*, 377–381.
- Muala, A.; Sehlstedt, M.; Bion, A.; Österlund, C.; Bosson, J.A.; Behndig, A.F.; Pourazar, J.; Bucht, A.; Boman, C.; Mudway, I.S.; et al. Assessment of the capacity of vehicle cabin air inlet filters to reduce diesel exhaust-induced symptoms in human volunteers. *Environ. Health* **2014**, *13*, 16.
- ASHRAE. Ventilation for Acceptable Indoor Air Quality, ANSI/ASHRAE Standard 62.1. American National Standards Institute and American Society of Heating, Refrigerating and Air-Conditioning Engineers. 2016. Available online:

- <https://www.ashrae.org/technical-resources/standards-and-guidelines/read-only-versions-of-ashrae-standards> (accessed on 26 July 2021).
23. Health Canada. Residential Indoor Air Quality Guidelines for Carbon Dioxide— for Public Consultation. 2020. Available online: <https://www.canada.ca/en/health-canada/programs/consultation-residential-indoor-air-quality-guidelines-carbon-dioxide/document.html> (accessed on 26 July 2021).
 24. Grady, M.L.; Jung, H.; Kim, Y.C.; Park, J.K.; Lee, B.C. Vehicle cabin air quality with fractional air recirculation. *SAE Tech. Pap.* **2013**, <https://doi.org/10.4271/2013-01-1494>.
 25. Tartakovsky, L.; Baibikov, V.; Czerwinski, J.; Gutman, M.; Kasper, M.; Popescu, D.; Veinblat, M.; Zvirin, Y. In-vehicle particle air pollution and its mitigation. *Atmos. Environ.* **2013**, *64*, 320–328.
 26. Brown, R.C. Electrically charged air filterst. *KONA Powder Part. J.* **1991**, *9*, 174–186.
 27. Ardkapan, S.R.; Johnson, M.S.; Yazdi, S.; Afshari, A.; Bergsøe, N.C. Filtration efficiency of an electrostatic fibrous filter: Studying filtration dependency on ultrafine particle exposure and composition. *J. Aerosol Sci.* **2014**, *72*, 14–20.
 28. Maricq, M.M.; Podsiadlik, D.H.; Chase, R.E. Gasoline vehicle particle size distributions: Comparison of steady state, FTP, and US06 measurements. *Environ. Sci. Technol.* **1999**, *33*, 2007–2015.
 29. Harris, S.J.; Maricq, M.M. Signature size distributions for diesel and gasoline engine exhaust particulate matter. *J. Aerosol Sci.* **2001**, *32*, 749–764.
 30. Kittelson, D.B.; Watt, W.F.; Johnson, J.P. On-road and laboratory evaluation of combustion aerosols-part 1: Summary of diesel engine results. *J. Aerosol Sci.* **2006**, *37*, 913–930.
 31. Kittelson, D.B.; Watt, W.F.; Johnson, J.P.; Schauer, J.J.; Lawson, D.R. On-road and laboratory evaluation of combustion aerosols-part 2: Summary of spark ignition engine results. *J. Aerosol Sci.* **2006**, *37*, 931–949.
 32. Chan, T.W.; Meloche, E.; Kubsh, J.; Rosenblatt, D.; Brezny, R.; Rideout, G. Evaluation of a gasoline particulate filter to reduce particle emissions from a gasoline direct injection vehicle. *SAE Int. J. Fuels Lubr.* **2012**, *5*, 1277–1290, doi:10.4271/2012-01-1727.
 33. Chan, T.W.; Meloche, E.; Kubsh, J.; Brezny, R. Black carbon emissions in gasoline exhaust and a reduction alternative with a gasoline particulate filter. *Environ. Sci. Technol.* **2014**, *48*, 6027–6034.
 34. Saffaripour, M.; Chan, T.W.; Liu, F.; Thomson, K.A.; Smallwood, G.J.; Kubsh, J.; Brezny, R. Effect of drive cycle and gasoline particulate filter on the size and morphology of soot particles emitted from a gasoline-direct-injection vehicle. *Environ. Sci. Technol.* **2015**, *49*, 11950–11958.
 35. Calcote, H.F. Mechanisms of soot nucleation in flames—A critical review. *Combust. Flame* **1981**, *42*, 215–242.
 36. Onischuk, A.A.; di Stasio, S.; Karasev, V.V.; Strunin, V.P.; Baklanov, A.M.; Panfilov, V.N. Evidence for long-range Coulomb effects during formation of nanoparticle agglomerates from pyrolysis and combustion routes. *J. Phys. Chem. A* **2000**, *104*, 10426–10434.
 37. Onischuk, A.A.; di Stasio, S.; Karasev, V.V.; Baklanov, A.M.; Makhov, G.A.; Vlasenko, A.L.; Sadykova, A.R.; Shipovalov, A.V.; Panfilov, V.N. Evolution of structure and charge of soot aggregates during and after formation in a propane/air diffusion flame. *J. Aerosol Sci.* **2003**, *34*, 383–403.
 38. Baumgartner, H.P.; Löffler, F. The collection performance of electret filters in the particle size range 10 nm–10 µm. *J. Aerosol Sci.* **1986**, *17*, 438–445.
 39. Walsh, D.C.; Stenhouse, J.I.T. The effect of particle size, charge, and composition on the loading characteristics of an electrically active fibrous filter material. *J. Aerosol Sci.* **1997**, *28*, 307–321.
 40. Walsh, D.C.; Stenhouse, J.I.T. Parameters affecting the loading behavior and degradation of electrically active filter materials. *Aerosol Sci. Technol.* **1998**, *29*, 419–432.
 41. Jing, L. Standard combustion aerosol generator (SCAG) for calibration purposes. In Proceedings of the 3rd ETH Workshop “Nanoparticle Measurement”, Zurich, Switzerland, 9–10 August 1999.
 42. Moore, R.H.; Ziemba, L.D.; Dutcher, D.; Beyersdorf, A.J.; Chan, K.; Crumeyrolle, S.; Raymond, T.M.; Thornhill, K.L.; Winstead, E.L.; Anderson, B.E. Mapping the operation of the Miniature Combustion Aerosol Standard (Mini-CAST) soot generator. *Aerosol Sci. Technol.* **2014**, *48*, 467–479.
 43. Johnson, T.; Caldow, R.; Pocher, A.; Mirme, A.; Kittelson, D. A new electrical mobility particle sizer spectrometer for engine exhaust particle measurements. *SAE Tech. Pap.* **2004**, <https://doi.org/10.4271/2004-01-1341>.
 44. Snelling, D.R.; Smallwood, G.J.; Sawchuk, R.A.; Neill, W.S.; Gareau, D.; Clavel, D.J.; Chippior, W.L.; Liu, F.; Gülder, Ö.L.; Bachalo, W.D. In-situ real-time characterization of particulate emissions from a diesel engine exhaust by laser-induced incandescence. *SAE Tech. Pap.* **2000**, <https://doi.org/10.4271/2000-01-1994>.
 45. Snelling, D.R.; Smallwood, G.J.; Liu, F.; Gülder, Ö.L.; Bachalo, W.D. A calibration-independent laser-induced incandescence technique for soot measurement by detecting absolute light intensity. *Appl. Opt.* **2005**, *44*, 6773–6785.
 46. Lehmann, U.; Niemelä, V.; Mohr, M. New method for time-resolved diesel engine exhaust particle mass measurement. *Environ. Sci. Technol.* **2004**, *38*, 5704–5711.
 47. Weichenthal, S.; Van Ryswyk, K.; Kulka, R.; Sun, L.; Wallace, L.; Joseph, L. In-vehicle exposures to particulate air pollution in Canadian metropolitan area: The urban transportation exposure study. *Environ. Sci. Technol.* **2015**, *49*, 597–605.
 48. Van Ryswyk, K.; Anastasopoulos, A.T.; Evans, G.; Sun, L.; Sabaliauskas, K.; Kulka, R.; Wallace, L.; Weichenthal, S. Metro commuter exposures to particulate air pollution and PM_{2.5}-associated elements in three Canadian cities: The Urban Transportation Exposure Study. *Environ. Sci. Technol.* **2017**, *51*, 5713–5720.

49. Austin, C.C.; Wang, D.; Ecobichon, D.J.; Dussault, G. Characterization of volatile organic compounds in smoke at municipal structural fires. *J. Toxicol. Environ. Health A* **2001**, *63*, 437–458.
50. Kittelson, D.B.; Dolan, D.F.; Verrant, J.A. Investigation of a diesel exhaust aerosol. *SAE Tech. Pap.* **1978**, 780109, <https://doi.org/10.4271/780109>.
51. McMurry, P.H.; Wang, X.; Park, K.; Ehara, K. The relationship between mass and mobility for atmospheric particles: A new technique for measuring particle density. *Aerosol Sci. Technol.* **2002**, *36*, 227–238.
52. Park, K.; Cao, F.; Kittelson, D.B.; McMurry, P.H. Relationship between particle mass and mobility for diesel exhaust particles. *Environ. Sci. Technol.* **2003**, *37*, 577–583.
53. Maricq, M.M.; Xu, N. The effective density and fractal dimension of soot particles from premixed flames and motor vehicle exhaust. *J. Aerosol Sci.* **2004**, *35*, 1251–1274.
54. Symonds, J.P.R.; Reavell, K.S.T.J.; Olfert, J.S.; Campbell, B.W.; Swift, S.J. Diesel soot mass calculation in real-time with a differential mobility spectrometer. *J. Aerosol Sci.* **2007**, *38*, 52–68.
55. Quiros, D.C.; Hu, S.; Hu, S.; Lee, E.S.; Sardar, S.; Wang, X.; Olfert, J.S.; Jung, H.S.; Zhu, Y.; Huai, T. Particle effective density and mass during steady-state operation of GDI, PFI, and diesel passenger cars. *J. Aerosol Sci.* **2015**, *83*, 39–54.
56. Stafford, R.G.; Ettinger, H.J. Filter efficiency as a function of particle size and velocity. *Atmos. Environ.* **1972**, *6*, 353–362.
57. Hanley, J.T.; Ensor, D.S.; Smith, D.D.; Sparks, L.E. Fractional aerosol filtration efficiency of in-duct ventilation air cleaners. *Indoor Air* **1994**, *4*, 169–178.